

We are IntechOpen, the world's leading publisher of Open Access books Built by scientists, for scientists

6,900

Open access books available

186,000

International authors and editors

200M

Downloads

Our authors are among the

154

Countries delivered to

TOP 1%

most cited scientists

12.2%

Contributors from top 500 universities



WEB OF SCIENCE™

Selection of our books indexed in the Book Citation Index
in Web of Science™ Core Collection (BKCI)

Interested in publishing with us?
Contact book.department@intechopen.com

Numbers displayed above are based on latest data collected.
For more information visit www.intechopen.com



Localized Excitation of Single Atom to a Rydberg State with Structured Laser Beam for Quantum Information

Leila Mashhadi and Gholamreza Shayeganrad

Abstract

Sufficient control over the excitation of the Rydberg atom as a quantum memory is crucial for the fast and deterministic preparation and manipulation of the quantum information. Considering the Laguerre-Gaussian (LG) beam spatial features, localized excitation of a four-level atom to a highly excited Rydberg state is presented. The position-dependent AC-Stark shift of the first and Rydberg state in the effective quadrupole two-level description of a far-detuned three-photon Rydberg excitation results in a steep trapping potential for Rydberg state. The transfer of optical orbital angular momentum from LG beam to the Rydberg state via quadrupole transition in the last Rydberg excitation process offers a long-lived and controllable qudit quantum memory. The effective quadrupole Rabi frequency is presented as a function of ratio of the first to Rydberg excitation laser beam waist and the center of mass position inside the trap. It depicts high accuracy of detecting Rydberg atom at the center of the trap, which can pave the way for implementation of high-fidelity qudit gate.

Keywords: Rydberg excitation, dipole-quadrupole trap, Laguerre-Gaussian beam, qudit

1. Introduction

1.1 Trapped neutral atom as quantum memories

Photons are ideal carrier of quantum information for communication, but storing them for a long time is difficult. In optical quantum communication, a quantum network can consist of spatially separated quantum memories to store and manipulate information which is encoded in internal quantum state of physical system such as photons, ions, atoms, etc. [1]. In order to operate a successful long-distance quantum communication and quantum information processing, the quantum memory should have a high-storage efficiency, which is defined as the ratio of input photon energy to long coherence time. Different physical systems such as cold atoms trapped in optical lattices [2–8] or cold ions in electrostatic traps [9] are used as quantum memories. Ions are electrically charged and therefore can be tightly confined in deep traps for a long time. However, the strong Coulomb repulsion

limits the number of ions that can be precisely controlled in a single trap. In contrast, more promising experiments could be made with the cold trapped neutral atoms. The neutral atoms usually interact only at very short range and can be collected in large ensembles without perturbing each other, and therefore the decoherence and losing the quantum information due to the interaction with the environment are low. In other words, single qubits [1] or even multi-qubits can be encoded in atomic states which afford long coherence times. Cooling and trapping of neutral atoms is one of the challenging techniques to achieve a higher signal-to-noise ratio and to stabilize the system over long periods for more balanced memory efficiency and fully control of all physical degrees of freedom with long coherence times. To keep the atom in trap, it is necessary to raise the atomic trap depth to be comparable to or even larger than the thermal energy of background atoms. Although, in principle, there is no fundamental limit to the lifetime with sufficiently deep traps, there are practical limitations. Optical traps for neutral atoms cannot be arbitrarily deep since both the trap depth and the photon scattering rate, which causes decoherence, scale proportional to the optical power. Even in the absence of collisional losses as the main reason to lose the trapped atom, the heating due to fluctuations of the trapping potential can eventually cause trapped atoms to escape. As a result, the trapping system used to confine the atoms is switched off during the storage. Nevertheless, the residual electric and magnetic field still limits the lifetime of the quantum memory [10, 11]. For a quantum memory in a magneto-optical trap (MOT), the atomic diffusion imposes a strict limitation on the storage time, which in turn limits the maximum distance for quantum communication in practical applications. On the contrary, the optical dipole trap can offer an array of spatial forms which can be rapidly switched as well [12]. Optical dipole traps rely on the induced atomic electric dipole interaction with electric component of the trapping light. The power needed for trapping depends on the desired trap depth and the detuning from the nearest optical transitions. Small detuning gives deeper traps, with a depth scaling as $1/\Delta$, where Δ is the detuning from the nearest strong electronic transition. This must be balanced against the photon scattering rate, which causes heating and decoherence and scales as $1/\Delta^2$ [13]. When the light frequency is far-detuned [12, 14, 15], a nearly conservative potential well with less influence from spontaneous photon scattering is created for the atom. The AC-Stark shift in the atomic state from the induced dipole gives sensitivity to intensity noise of lasers and atomic position. The nonuniform spatial intensity profile results in the intensity-dependent AC-Stark shift and defines the shape of associated atom trap. Therefore, the AC-Stark shift affects the qubit level, and fluctuation in laser field leads to broad the qubit line.

In red-detuned far-off resonance optical dipole trap (FORT) [16, 17], the laser beam is focused to attract atoms to the region, where the intensity is high. The large detuning efficiently suppresses the effect of scattered photons. On the other hand, the blue-detuned FORT [18, 19] can confine the atom in the dark region of the blue-detuned laser beams. The blue-detuned FORT has several advantages over the bright trap of the red-detuned laser. As the atoms are trapped in the “dark” place, the photon scattering rate due to the trapping laser can be greatly reduced, while in the bright trap, this rate can be reduced only by increasing the detuning of the trapping laser. A quantum memory of this sort thus has a potential storage time of seconds [13]. In conclusion all the abovementioned issues, such as linear and nonlinear scattering, recoil heating, intensity fluctuation, and pointing instabilities of the trapping beams, result in dipole-force fluctuations, and collisions with the background gas lead to heating up the qubit atom and therefore escaping from the trap [20]. This motivates the researchers to look for a way to create more stable quantum memories with longer storage time.

1.2 Rydberg atoms for quantum information

The optical degrees of freedom of single atoms such as polarization, wavelength, transverse mode, etc., can provide qubits or qudits for quantum information. Thus control and manipulation of single atoms are now of great interest given the potential to create quantum registers with single-atom techniques [21–24]. Furthermore, the observation of entanglement between a single atom and a single photon [25] provides the precondition for quantum communication and computation. Ground atomic states are ideal for preserving quantum coherence [26], but implementation of fast and deterministic quantum operations is challenging due to their weak interactions. Such considerations suggest to employ a quantum superposition of a ground and a Rydberg state to achieve both fast and deterministic quantum operations and long-lived memory [27]. A Rydberg atom is an atom in a highly excited state, typically with a principal quantum number $n \gg 1$. The excited valence electron can travel microns from the nucleus, while still remaining bound to it. Because the Rydberg electron is so far from the core of the atom, the Rydberg atom develops exaggerated properties, such as high polarizability. The strong dipolar interactions between Rydberg atoms can potentially be used for fast quantum gates between qubits stored in stable ground states of neutral atoms [28, 29]. The electric dipole strength of highly excited Rydberg atoms results in the Rydberg excitation blockade [28–33] which can be used in combination with electromagnetically induced transparency (EIT) [34, 35] to generate quantum states of light, entanglement of several atoms, and quantum logic gates [36–38]. The mapping of Rydberg interactions onto photons by means of EIT has emerged as a powerful approach to realizing few-photon optical nonlinearities [39–41] and provides the possibility to control the interaction between photons, which is a key ingredient to the goal of quantum information processing. Due to the nature of Rydberg blockade, the Rydberg nonlinearity is a sufficiently large and long range to build an optical quantum computer. The possibility to coherently control the quantum state of photon via dark-state Rydberg polaritons opens up interesting applications in reversible quantum memories for light waves [42] and shall find a possibility for a fast transformation [43].

1.3 Structured laser beam and atom

The development of structured laser beams such as Laguerre-Gaussian (LG) beams has enabled the coherent production of large number of identical spiral photons [44–47], which opens a new set of research in quantum optics in atomic level. LG beams are characterized by three quantum numbers: (i) the wave number k , (ii) the intertwined helical wave fronts l (an integer number) of azimuthal phase-dependent that features a screw dislocation, and (iii) the radial nodes p [48, 50]. Each spiral photon in the LG beams carries $l\hbar$ of intrinsic orbital angular momentum (OAM) along the direction of propagation [51], which is arising from their nonuniform spatial intensity distribution. The characteristic shape of the intensity distribution of LG beams as well as their intrinsic orbital angular momentum can be observed as a result of this interaction. The exchange of angular momentum induces a torque and an azimuthal shift in the resonant frequency besides the usual axial Doppler shift and recoil shift which tailored the control of the motion of the center of mass of the atoms to rotate about the beam axis [52, 53]. In higher order quadrupole transition processes, the internal motion of the atom participates in orbital angular momentum exchange between structured light and atom [54–57]. However, in dipole transition, the interaction of LG beam with atom and therefore

transferring of OAM from LG beam to the external degree of freedom of the atom presents in the quantization of the center of mass motion of the atom [58].

A Rydberg atom with near classical size comparable to the wavelength of photon is big enough to feel phase differences of the helical wave front of LG beams. The LG beam has an advantage of control and narrows the resonances in electromagnetically induced transparency. The orbital angular momentum of LG beams has emerged as a popular choice for experiments on high-dimensional quantum information [59]. The dark center of blue-detuned Laguerre-Gaussian beam is emerged as an important feature to trap neutral atoms to decrease the atomic heating and decoherence rates and minimize the AC-Stark shift [60, 61]. In quantum information processing and data transmission, optical orbital angular momentum of spiral photons can provide an extra degree of entanglement [48] to carry quantum information in the different degrees of freedom by the higher dimensionality of the Hilbert space. In other words, the information carried by each photon can be increased significantly, from a qubit to a qudit, where d is the number of orthogonal basis vectors of the Hilbert space in which the photon lives.

1.4 Rydberg excitation

The excitation of a trapped neutral atom to a highly excited Rydberg state with long coherent time of ground-Rydberg transition is a promising platform for fast multi-qubit gates. The Rydberg state lifetime must be taken into account since the Rydberg state needs to be populated in order to implement two-qubit logical operations. The elementary operations necessary with Rydberg atoms in quantum information rely on the ability to coherently excite a Rydberg state and then returning them back to the ground state in controlled way so that the Rydberg atom is available for further processing. The lack of widely tunable frequency-stabilized ultraviolet wavelength diode lasers required for the direct excitation from the ground state to Rydberg states as well as weak direct excitation cross section has led to the use of multistep processes involving visible and near-infrared wavelengths [62–64]. To limit the spontaneous emission from the intermediate states in multistep excitation, which destroys the coherence, the population of the intermediate states can be manipulated by enlarging the detuning of the excitation laser frequency from the respective resonance frequency compared to the Rabi frequency of single-photon excitation. For large enough detunings, the intermediate states can be eliminated and a four-level system can be approximated to a two-level system with a total coupling strength. In this case, to obtain coherent coupling between the ground state and the Rydberg state, it is necessary to achieve an effective Rabi-frequency Ω well larger than the linewidth of the Rydberg state or of the driving laser fields. The coherent excitation of individual atoms trapped in tight optical dipole using two-photon excitation process has recently been described [65–68]. Also in order to cancel Doppler and recoil effects in Rydberg excitation, which limit the fidelity of the quantum gate [69], three-photon Rydberg excitation configuration is already proposed [70]. However, selectively localized and coherent excitation of atom to a highly excited Rydberg state and creation of a perfect blockade are still challenging [3, 71]. Firstly, the common red-detuned dipole traps can store atoms in the ground state with low decoherence, but they do not trap Rydberg states, and moreover, an atom in the Rydberg state moves in different optical potential than that experienced by the ground state. Secondly, the photo-ionization near the core due to the red-detuned trapping light, the sensitivity to the stray fields because of the large electron orbit and large polarizability that scales as $\propto n^7$ [72], and the motional-induced dephasing presents crucial limits to the usable spectrum. Thirdly, although the intermediate state detuning reduces spontaneous

emission, however, the small spontaneous emission besides of atomic motion and collisions [73] can limit storage times and therefore the ground-Rydberg atomic coherence time. Fourthly, the weak oscillator strength between ground and highly excited Rydberg state and very large electric dipole requires high laser excitation intensity to achieve the required signal-to-noise ratio. Fifthly, in most implementations using lattices or trap arrays generated with diffractive optics, it is relatively difficult to control the trap intensity and avoid perturbation of the atomic energy levels induced by inhomogeneous light distributions. Finally, in highly excited state, the energy separation is very small so that the selective excitation of the atom to a highly excited Rydberg state requires experimental technique with extremely high resolution.

To reduce errors in Rydberg excitation experiments, one solution is turning off the trapping system before the Rydberg excitation. However, it can cause problem for implementations with many qubits and creates unwanted Doppler shifts. This can be addressed by choosing a trap that works for both ground and Rydberg state of the atom. On the other hand, for the implementation of Rydberg-based quantum computing protocols with neutral atoms [3, 74–76], one can use a magic wavelength at which two atomic states (ground and Rydberg states) experience the same AC-Stark shift in a light field. In this chapter, a four-level Rydberg atom as a quantum memory in far-off resonance optical dipole-quadrupole trap is introduced. The controlling of the quantum state of localized Rydberg atom by tuning the excitation parameters is presented. It is shown that the ability to control the quantum state of Rydberg atom opens some interesting prospects for advances in quantum information processing.

2. High precision excitation and manipulation of a localized single atom to a highly excited Rydberg state

In this section, the theory of the three-step axial Doppler-free GGLG excitation of an alkali atom (e.g., Rb) from the ground state to the desired Rydberg state at the level of a single atomic excitation which is crucial for applications to quantum information processing is presented. The Rydberg excitation process is based on far-off resonance dipole-dipole-quadrupole transition. The quadrupole Rydberg transition in the last step is via LG-polarized laser beam. The Rydberg atom is localized at the dark center of structured beam, where the effect of atomic vibrations as well as AC-Stark shift is completely disappeared. The geometry of excitation as well as unique properties of LG-Rydberg excitation beam provides qudit of quantum memory in less disrupting effects such as motional heating effect, spontaneous emission due to high power, AC-Stark and Doppler, and recoil shift at the center of the trap which guarantee the high-fidelity gate.

2.1 Excitation configuration

The schematic diagram of a four-level atomic system is shown in **Figure 1**. We denote $|0\rangle$ to be the atomic ground state and $|i\rangle$ with $i = 1, 2, 3$ to be the respective first, second, and third excited states separated by energy $E_i - E_{i-1}$. The atom is cooled down to the recoil temperature and localized at the intersecting point of the excitation laser beams in the transversal plane $z = 0$ as sketched in **Figure 2(a)**. The wave vectors \mathbf{k}_i , $i = 1, 2, 3$, lie in x - z surface with the z axis directed along the LG-Rydberg excitation laser beams wave vector, \mathbf{k}_3 . While the first and second Gaussian excitation laser beams wave vectors, \mathbf{k}_1 and \mathbf{k}_2 , have the respective incidence angles θ_1 and

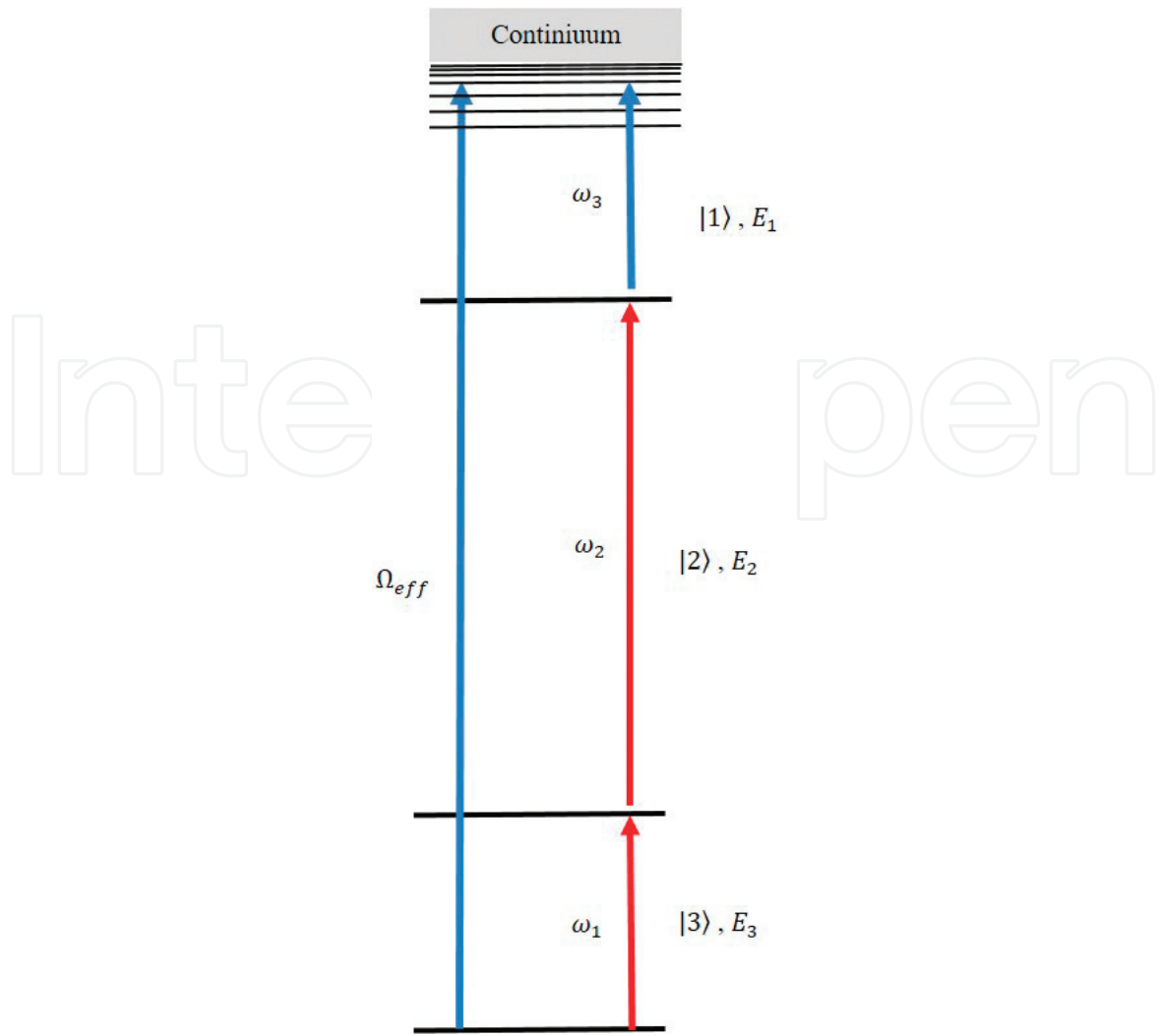


Figure 1.
Energy-level diagram three-photon Rydberg excitation [77].

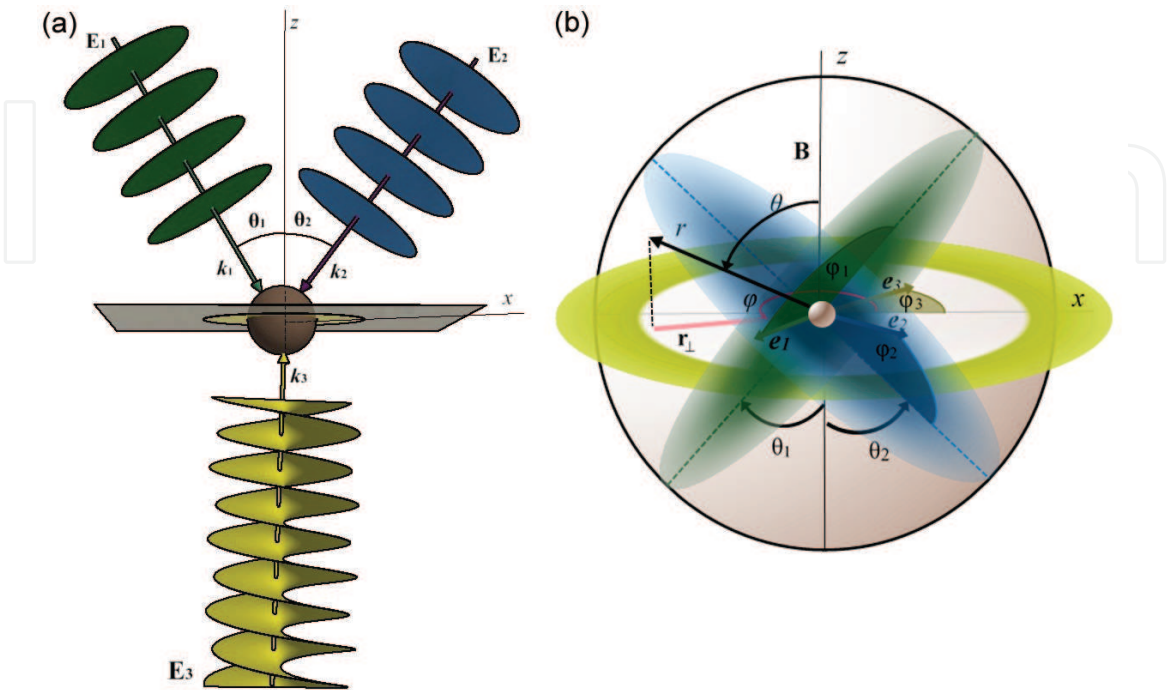


Figure 2.
(a) Geometry of Rydberg excitation via three-photon dipole-dipole-quadrupole transition. (b) Details of vectors and quantities involving in the excitation process [77].

θ_2 to the z axis. As it is explained in the following section, this special geometry provides the possibility for Doppler and recoil-free excitation.

The Rydberg atom-field interaction considered here corresponds to situations, where firstly the Rydberg atom's size is comparable to the LG-beam waist in the third Rydberg excitation and the Rydberg electron sees the variation of the light intensity. Different parts of the atom can feel different electric fields, and the quadrupole transition, which seems to be negligible in most situations due to a much stronger simultaneous effect of the dipole one, is considerably increased. Secondly, the Rydberg and two intermediate states decay by spontaneous emission, and it is assumed that the lifetime of the Rydberg state is much longer than the other states, and so its decay can be neglected during the time scales relevant to the excitation process. Finally, the dipole-dipole interaction between the Rydberg atoms, which may induce the blockade, is omitted to focus on the single-atom excitation mechanism.

2.2 Excitation laser beams

The four-level atom is driven by three laser fields, the Gaussian first and second excitation laser field with respective frequency ω_1 and ω_2 and the LG-Rydberg excitation laser field with frequency ω_3 . Neglecting the focusing and the radial complexity and the mode curvature of the excitation laser beams, the electric field of each one-photon transition in the cylindrical-polar coordinates is given by

$$\mathbf{E}_{1,2}(R_{\perp}, \Phi, Z) = \mathbf{e}_{1,2} E_{01,2} f_{G1,2}(R_{\perp}) e^{i(\Theta_{1,2}(\mathbf{R}))}, \quad (1)$$

$$\mathbf{E}_{\ell p}(R_{\perp}, \Phi, Z) = \mathbf{e}_3 E_{03} \xi_{\ell p} \left(\frac{\sqrt{2}}{w_{03}} \right)^{|\ell|} f_{LG3}(R_{\perp}) e^{i(\Theta_3(\mathbf{R}))}, \quad (2)$$

where

$$f_{G1,2}(R_{\perp}) = e^{-\frac{R_{\perp}^2}{w_{01,2}^2}}, \quad (3)$$

$$f_{LG3}(R_{\perp}) = R_{\perp}^{|\ell|} e^{-\frac{R_{\perp}^2}{w_{03}^2}} L_p^{|\ell|} \left(\frac{2R_{\perp}^2}{w_{03}^2} \right), \quad (4)$$

$$\Theta_{1,2}(\mathbf{R}) = \mathbf{k} \cdot \mathbf{R}, \quad (5)$$

and

$$\Theta_3(\mathbf{R}) = \ell\varphi + \mathbf{k}_3 \cdot \mathbf{R}. \quad (6)$$

Here \mathbf{e}_i , w_{0i} , and \mathbf{k}_i are the polarization, beam waist at $z = 0$, and wave vector of the i th excitation laser field, respectively. The electric field amplitudes E_{0i} are connected to the laser intensity I_i via $E_{0i} = \sqrt{(2I_i/c\epsilon_0)}$, where c is the speed of light and ϵ_0 is the vacuum permittivity. In Eq. (2), ℓ corresponds to the optical orbital angular momentum, the mode index p represents the number of radial nodes of LG beam, $\xi_{\ell p} = \sqrt{\frac{2p!}{\pi(p+|\ell|)}}$ is the normalization constant, and $L_p^{|\ell|}$ is the Laguerre polynomial. The last excitation LG beam propagating along the z-direction in the plane of the focus of the beam appears as rings with radius R_l that is scaled linearly to the optical angular momentum and proportional to the beam waist [78]. The polarization \mathbf{e}_i determines the particular transition conditions happened in i th laser beam. The appearance of the polarization vector \mathbf{e}_i depends explicitly upon the choice of

coordinate orientation. In the basis of \mathbf{e}_σ , where $\sigma = \{1, -1, 0\}$ corresponds to the right circular, left circular, and linear polarization vector attached to the quantization axis z in xyz frame, the \mathbf{e}_i are given by

$$\mathbf{e}_i(\theta_i, \varphi_i) = \sum_{\sigma} s_{i\sigma}(\theta_i, \varphi_i) \mathbf{e}_\sigma, \quad (7)$$

where $s_{i\sigma}(\theta_i, \varphi_i)$ is the relation coefficient and φ_i is the azimuthal angle of respective polarization according to **Figure 2(b)**.

The i th laser excitation beam carries linear momentum $\hbar \mathbf{k}_i$, and spin angular momentum $\pm \hbar$ per photon relates to the excitation laser polarization, if circularly polarized, while the last LG beam with an azimuthal phase dependence $\exp(il\phi)$ in addition to linear and spin angular momentum carries orbital angular momentum that can be many times greater than the spin [49]. The combination of energy selectivity, associated with the laser light frequency, and sublevel selectivity, associated with polarization as well as angular momentum of light beam, provides good controls and manipulation over the qudits in quantum information processing.

2.3 The interaction of a four-level atom with three excitation laser fields

Let us begin with the four-level atom introduced in **Figure 1**. In general, the state of the atom for the coupled atom-laser system can be written in terms of the eigenstates of H_{atom} , the unperturbed Hamiltonian for the atomic system in the absence of the excitation laser, as

$$|\psi(\mathbf{r}, t)\rangle = c_0(t)\psi_0(\mathbf{r})e^{-i\frac{E_0}{\hbar}t}|0\rangle + \sum_i c_i(t)\psi_i(\mathbf{r})e^{-i\frac{E_i}{\hbar}t}|i\rangle, \quad (8)$$

where c_i ($i = 0, 1, 2, 3$) is the probability amplitude of i th state. The Hamiltonian for the system can be taken as

$$\widehat{H} = \widehat{H}_{\text{atom}} + \widehat{H}_{\text{int}}, \quad (9)$$

where $\widehat{H}_{\text{int}} = \widehat{H}_d + \widehat{H}_q$,

where $\mathbf{E}(R_\perp, \Phi, Z) = \mathbf{E}_1(R_\perp, \Phi, Z) + \mathbf{E}_2(R_\perp, \Phi, Z) + \mathbf{E}_{3lp}(R_\perp, \Phi, Z)$ is the total electric field of excitation lasers, and where \widehat{H}_d and \widehat{H}_q are the coupling to the electric dipole and quadrupole moment, respectively [79]. The first two excitations proceed via dipole transition employing the first two Gaussian laser beams, while the Rydberg excitation takes place through the quadrupole transition using the polarized LG beam.

To study the dynamics of the population of the different levels of the atom, we need to know $c_i(t)$ by solving the Schrodinger equation:

$$i\hbar \frac{\partial}{\partial t} |\psi(\mathbf{r}, t)\rangle = \widehat{H}' |\psi(\mathbf{r}, t)\rangle, \quad (10)$$

where

$$\widehat{H}' = \widehat{U}\widehat{H}\widehat{U}^{-1} + -i\hbar \widehat{U} \frac{\partial}{\partial t} \widehat{U}^{-1}. \quad (11)$$

In matrix notation, the Schrodinger equation after rotating wave approximation can be given by

$$\frac{\partial}{\partial t} \begin{pmatrix} c_0(t) \\ c_1(t)e^{i\Delta_1 t} \\ c_2(t)e^{i(\Delta_2+\Delta_1)t} \\ c_3(t)e^{i\Delta t} \end{pmatrix} = -i \begin{pmatrix} 0 & \frac{\Omega_1}{2} & 0 & 0 \\ \frac{\Omega_1}{2} & \Delta_1 & \frac{\Omega_2}{2} & 0 \\ 0 & \frac{\Omega_2}{2} & \Delta_1 + \Delta_2 & \frac{\Omega_3}{2} \\ 0 & 0 & \frac{\Omega_3}{2} & \Delta \end{pmatrix} \begin{pmatrix} c_0(t) \\ c_1(t)e^{i\Delta_1 t} \\ c_2(t)e^{i(\Delta_2+\Delta_1)t} \\ c_3(t)e^{i\Delta t} \end{pmatrix}. \quad (12)$$

Here

$$\Omega_{1,2}(R_\perp) = \left(\frac{2e^2 I_{1,2}}{\hbar^2 c \epsilon_0} \right)^{\frac{1}{2}} \mathbf{r}_{0,1 \rightarrow 1,2} \cdot \mathbf{e}_{1,2}(\theta_{1,2}, \varphi_{1,2}) f_{G1,2}(R_\perp) \quad (13)$$

and

$$\Omega_3(R_\perp) = \left(\frac{2e^2 I_3}{\hbar^2 c \epsilon_0} \right)^{\frac{1}{2}} \frac{2r_\perp \mathbf{r}_{2 \rightarrow 3}}{\sqrt{\pi} \omega_{03}} \cdot \mathbf{e}_3(\theta_3, \varphi_3) e^{i\varphi} \frac{d}{dR_\perp} f_{LG3}(R_\perp) \quad (14)$$

are the first and second dipole and the last quadrupole Rydberg excitation Rabi frequencies, respectively, where $\mathbf{r}_{i-1 \rightarrow i} = \langle i-1 | \boldsymbol{\psi}_{i-1}^*(\mathbf{r}) \mathbf{r} \boldsymbol{\psi}_i(\mathbf{r}) | i \rangle$ stand for the atomic dipole momentums between states $i-1$ and i , with respective eigenfunctions $\boldsymbol{\psi}_{i-1}(\mathbf{r})$ and $\boldsymbol{\psi}_i(\mathbf{r})$; $\Delta_i = \omega_i - \frac{E_i - E_{i-1}}{\hbar} + \Delta_{iD}$ is the detuning of state i affected by residual Doppler shifts:

$$\Delta_{iD} = \Theta_i \cdot \mathbf{v}_i \quad (15)$$

due to the random very small displacements and vibrations of the atom (see Eqs. (3) and (4)), even though the atom is cooled and trapped at the center of the LG beam, and $\Delta = \sum_{i=1}^3 \Delta_i = E_3 - E_0 - \sum_i \omega_i$ stands for the total detuning to the Rydberg state.

According to Eq. (14), the quadrupole Rabi frequency of the Rydberg excitation step in addition to the polarization depends on the orbital angular momentum of the LG beam. The phase factor $e^{i\varphi}$ changes the parity symmetry and transfers one unit of optical orbital angular momentum to the internal motion of atom. The quadratic radial, $r_\perp \mathbf{r}_{2 \rightarrow 3}$, in Eq. (14) is the consequence of the transversal variation of the LG-beam intensity.

2.3.1 Doppler and recoil shift compensation

The axial Doppler shift of the first, second, and Rydberg states by inserting Eqs. (3) and (4) in Eq. (14) can be, respectively, given as

$$\begin{aligned} \Delta_{1D} &= -k_1 v_1 \cos \theta_1 + k_1 v_1 \sin \theta_1, \\ \Delta_{2D} &= -k_2 v_2 \cos \theta_2 - k_2 v_2 \sin \theta_2, \\ \Delta_{3D} &= k_3 v_3 + \Delta_{LG}. \end{aligned} \quad (16)$$

It is noticeable that Δ_{3D} contains the azimuthal Doppler shift [80], $\Delta_{LG} = \frac{v_\Phi}{R_\perp}$, in addition to the axial Doppler shift, where v_Φ is the azimuthal velocity of the atom.

Doppler broadening due to atomic motion leads to imperfect Rydberg excitation which limits the fidelity of the entanglement that is created using Rydberg interactions. By adjusting θ_i , it is possible to get rid of the recoil and axial Doppler shift. According to **Figure 2(a)**, the excitation is recoil-free when

$$k_1 \sin \theta_1 = k_2 \sin \theta_2. \quad (17)$$

By substituting Eqs. (5) and (6) into Eq. (16), it is found that this flexible geometry of the excitation system results in the axial Doppler-free excitation condition in which the total detuning Δ is independent from the atomic vibrations but not rotations.

2.3.2 Adiabatic approximation and effective two-level transition

With the presence of decoherency, the evolution of the atomic states in memoryless environment will be expressed as density matrix formalism [81]. However, storing quantum information for long periods needs a decoherence-free quantum memory. In order to have coherent excitation, the spontaneous photon scattering should be limited by far detuning of laser excitation frequency from the respective excited state. In the limit of very large intermediate detuning such that, $|\Delta_i| \gg \Omega_i$ and $|\Delta_i| \gg |\Delta|$, the population of intermediate states is very low, and the system can behave as a two-level system with an effective coupling between ground and Rydberg states [77]. Supposing that the atom is initially in the ground state $|0\rangle$, the time dependence of the Rydberg state population by the GGLG-beam excitation scheme can be obtained from Eq. (12) as

$$|c_3|^2 = \frac{\Omega_{eff}^2}{\Omega_{eff}^2 + \Delta_{eff}^2} \sin^2 \left(\sqrt{\Omega_{eff}^2 + \Delta_{eff}^2} t \right), \quad (18)$$

where

$$\Delta_{eff}(R_{\perp}) = \Delta + \frac{\Omega_3^2(R_{\perp})}{4\Delta_3} + \frac{\Omega_1^2(R_{\perp})}{4\Delta_1} + \Delta_{LG}, \quad (19)$$

and

$$\Omega_{eff}(R_{\perp}) = \frac{\Omega_1(R_{\perp})\Omega_2(R_{\perp})\Omega_3(R_{\perp})}{4\Delta_1\Delta_3} \quad (20)$$

are the effective detuning and resonant Rabi frequency characterizing effective quadrupole coupling between ground and Rydberg states due to the dipole-dipole-quadrupole transition under the adiabatic approximation.

The transverse profile of three-photon GGLG effective quadrupole Rabi frequency has a narrow central peak compared to the one-photon quadrupole LG Rabi frequency without any sidelobe. Then, according to Eq. (18), the nonzero excitation probability is limited to the position of a single atom which is localized at the center of the trap leading to enhancement of the high-accuracy single-atom excitation.

2.3.3 Transition selection rules

To coherently excite a single atom to a Rydberg state for quantum information processing, it is crucial to determine the strength of the radial and angular momentum couplings between the ground and Rydberg states. Moreover, the quantum

qudit encoding is based on the spin and orbital angular momentum exchange in the interaction of atom with excitation laser beams, which is expressed in angular momentum coupling term. The internal atomic wave function in spherical polar coordinate is written as

$$\psi_{nlm}(\mathbf{r}) = u_{nl}(r)Y_{lm}(\theta, \varphi), \quad (21)$$

where $u_{nl}(r)$ is the radial part of the electron wave function, which for a Rydberg state can be approximated using quantum defect theory [82], and n , l , and m are quantum numbers, which characterize the atom states. Substituting Eq. (21) into Eqs. (13) and (14) and considering the polarization orientation with respect to the quantization axis, the Rabi frequency of each transition can be given by

$$\Omega_1(0) = \left(\frac{8\pi I_1}{3\hbar^2 \varepsilon_0 c} \right)^{\frac{1}{2}} eR_{n_0 l_0 \rightarrow n_1 l_1}(r) \sum_{\sigma} s_{1\sigma}(\theta_1, \varphi_1) \int_0^{2\pi} \int_0^{\pi} \sin \theta d\theta d\varphi Y_{l_0}^{m_0} * Y_1^{\sigma} Y_{l_1}^{m_1} \quad (22)$$

$$= \left(\frac{2I_1}{\hbar^2 \varepsilon_0 c} \right)^{\frac{1}{2}} eR_{n_0 l_0 \rightarrow n_1 l_1}(r) \beta_{1dp}$$

$$\Omega_2(0) = \left(\frac{8\pi I_2}{3\hbar^2 \varepsilon_0 c} \right)^{\frac{1}{2}} eR_{n_1 l_1 \rightarrow n_2 l_2}(r) \sum_{\sigma} s_{2\sigma}(\theta_2, \varphi_2) \int_0^{2\pi} \int_0^{\pi} \sin \theta d\theta d\varphi Y_{l_1}^{m_1} * Y_1^{\sigma} Y_{l_2}^{m_2} \quad (23)$$

$$= \left(\frac{2I_2}{\hbar^2 \varepsilon_0 c} \right)^{\frac{1}{2}} eR_{n_1 l_1 \rightarrow n_2 l_2}(r) \beta_{2dp}$$

$$\Omega_3(0) = \left(\frac{8\pi I_3}{3\hbar^2 \varepsilon_0 c} \right)^{\frac{1}{2}} \sqrt{\frac{32}{3}} \frac{eR_{n_2 l_2 \rightarrow n_3 l_3}(r)}{w_3} \sum_{\sigma} s_{3\sigma}(\theta_3, \varphi_3) \int_0^{2\pi} \int_0^{\pi} \sin \theta d\theta d\varphi Y_{l_2}^{m_2} * Y_1^{\sigma} Y_1^{\sigma} Y_{l_3}^{m_3}$$

$$= \left(\frac{16I_3}{\pi \hbar^2 \varepsilon_0 c} \right)^{\frac{1}{2}} \frac{eR_{n_2 l_2 \rightarrow n_3 l_3}(r)}{w_{03}} \beta_{3qp} \quad (24)$$

where $R_{n_{i-1}, l_{i-1} \rightarrow n_i, l_i}$ represent the overlap integral between the radial wave functions of the electron and the dipole-quadrupole moment and $\beta_{l_{i-1} m_{i-1} \rightarrow l_i m_i}$ are the angular coupling expressed in terms of Clebsch-Gordan coefficients [77].

$\beta_{l_{i-1} m_{i-1} \rightarrow l_i m_i}$ contributes in precise quadrupole Rydberg excitation with elemental parameters θ_i and Φ_i . Different combinations of θ_i and Φ_i provide all possible transitions accessible, which is applicable in precision measurements [83]. In case of $\theta_3 = 0$ as shown in **Figure 2(a)**, for left and right circularly polarized LG beam with $p = 0$ and $\ell = 1$, the angular momentum transferred to the internal motion of the Rydberg atom via quadrupole transition is $|\Delta m| = 2$ and 0 , respectively. Therefore, there is a possibility for the Rydberg atom to gain two units of angular momentum due to the quadrupole LG excitation: one from the polarization and the other from optical orbital angular momentum of LG beam. Additionally, the radial overlap integral of the quadrupole transition $R_{n_2 l_2 \rightarrow n_3 l_3}(r)$ is considerable for high-lying Rydberg state with respect to w_{03} , which increases the quadrupole Rabi frequency. Moreover, the w_{03} -dependence of the Rydberg excitation Rabi frequency reflects the fact that the electric quadrupole transitions for an LG beam scales with w_{03} (compared to the plane wave, which scales with wave number k). Therefore, a relevant focusing with respect to the diffraction limit in addition to sufficient LG-beam power enhances the probability of the effective quadrupole excitation.

2.3.4 Localized Rydberg excitation in dipole-quadrupole potential landscape

Considering red- and blue-far-off resonance detuned first, second, and Rydberg excitation laser beams, respectively, due to the position-dependent AC-Stark shift of ground and Rydberg states as derived in Eq. (19), a position-dependent dipole-quadrupole potential landscape is found:

$$U_{\text{FORDQT}}(R_{\perp}) = U_{\text{LG3}} + U_{\text{G1}}, \quad (25)$$

where

$$U_{q\text{LG3}} = U_{03} \left(\frac{d}{dR_{\perp}} f_{\text{LG3}}(R_{\perp}) \right)^2, \quad (26)$$

and

$$U_{d\text{G1}} = -U_{01} f_{\text{G1}}^2(R_{\perp}) \quad (27)$$

are the optical quadrupole and dipole potentials, respectively. In these expressions $U_{03} = \frac{\hbar}{4} \frac{|\Omega_3(0)|^2}{|\Delta_3(\mathbf{R}, \mathbf{V})|}$ and $U_{01} = \frac{\hbar}{4} \frac{|\Omega_1(0)|^2}{|\Delta_1(\mathbf{R}, \mathbf{V})|}$ are quadrupole and dipole potential depth. The first and the last excitation parameters are contributing in the self-trapping potential landscape called far-off resonance optical dipole-quadrupole trap (FORDQT), while the second deriving laser with high intensity increases the excitation probability. Turning the trap off also results in mechanical heating and decoherence due to entanglement between the qubit state and the center of mass motion. The far detuning from all atomic resonances substantially reduces the photon scattering rate, and the atom is localized in an almost conservative potential. It can be seen that the magnitude and direction of the force exerted on the atom depend on both the magnitude and sign of the intensity gradient and the detuning which pushes the atom back toward the dark center of the trap. The flexible geometry of the excitation configuration results in the axial Doppler- and recoil-free excitation at the center of the trap. The localized Rydberg excitation in FORDQT potential can pave the way to establish a new record for the length of the time that quantum information can be stored in and retrieved from a localized trapped Rydberg atom.

2.3.5 Optimization of the system by tuning the excitation parameters

The probability of coherent writing and reading a quantum state into and out of Rydberg atom as a long-lived memory depends on coherence time and strength of coupling between ground and Rydberg state. Substituting the Rabi frequencies defined in Eqs. (22)–(24) into Eqs. (19), (20) and (25), Δ_{eff} , Ω_{eff} , and U_{FORDQT} can be interpreted in terms of key parameters of excitation: the orientation of the excitation beams with respect to the quantum axis (θ_i), the intensity of laser excitation beams (I_i), the detuning from intermediate states (Δ_i), the laser polarization azimuthal angle (φ_i), and the orbital angular momentum and the beam waist of the Rydberg excitation LG beam. By adjusting θ_i the geometry of excitation can be constructed for a Doppler- and recoil-free excitation. The clever choice of φ_i results in the excitation to a desirable state. While Δ_i fulfills the far-off resonance condition, the intensity I_i can be adjusted to boost the effective quadrupole excitation with less effect of AC-Stark shift. Finally, the proper choice of excitation laser beam waists can result in a great reduction of trapping size. In the GGLG excitation

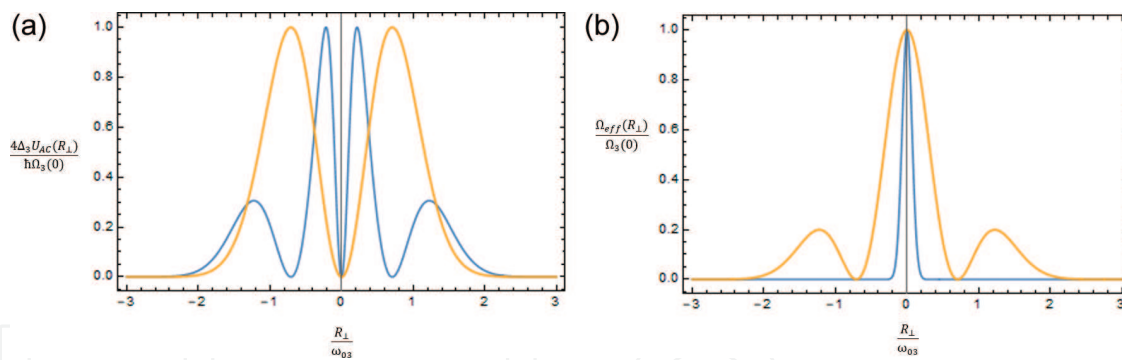


Figure 3. (a) The far-off resonance optical dipole-quadrupole trapping potential normalized to the quadrupole potential versus transversal position of center of mass of the Rydberg atom, for the case $\Omega_1 = \Omega_3$, $|\Delta_1| = |\Delta_3|$, and $\omega_{o1} = \omega_{o2} = 0.2 \omega_{o3}$ (blue line) [77].

process, the Rydberg atom confines in the FORDQT potential, which is sensitive to the Rydberg atom position with respect to the transversal variations of the intensity of the excitation lasers which keeps the Rydberg atom at the minimum noise position of the trapping center and thus controls localized qudit state in longer coherent time reasonable for quantum information processing. Comparing to the Rydberg dipole excitation via LG beam, the Rydberg GGLG excitation system localizes the atom in a much smaller region. According to **Figure 3**, if the LG beam is focused into some micron waist, then in this self-trapping excitation system, the atom can be excited to a Rydberg state while tightly confined and controlled to sub-micron dimensions. Consequently, in a high-dimensional quantum information experiments via Rydberg excitation, care should be taken to relative control over all these parameters.

3. Summary

In this chapter, the Doppler- and recoil-free three-photon GGLG excitation promises to extend a single localized atom to a highly excited Rydberg state, which has application in the control and transformation of high-dimensional quantum states [16]. The adiabatic approximation results in an effective quadrupole Rabi frequency with a rich geometrical dependency. The quadrupole interaction in the last step of the LG excitation transfers a unit of orbital angular momentum to the Rydberg state in addition to the spin angular momentum. The GGLG excitation system allows to greatly reducing the rate of photon scattering and suppresses the loss rate due to collision, while the trapping potential of FORODQT localizes the Rydberg excitation and increases excitation coherency and allows for high detection efficiency and long detection time. A wide range of properties characterizing the excitation configuration can be controlled in real time through changes in geometry, polarization and orbital angular momentum, focal spot size, intensity, and frequency of the laser excitation beams to provide the ability to encode qudit in the internal degree of freedom of Rydberg atom independently to the center-of-mass motion. This aspect is vital to store and manipulate the quantum state of qudits in high-dimensional quantum information processing.

IntechOpen

Author details

Leila Mashhadi^{1*} and Gholamreza Shayeganrad²

1 Independent Researcher, Basel, Switzerland

2 Department of Biomedical Engineering, University of Basel, Allschwil, Switzerland

*Address all correspondence to: leila.mashhadi@yahoo.com

IntechOpen

© 2019 The Author(s). Licensee IntechOpen. This chapter is distributed under the terms of the Creative Commons Attribution License (<http://creativecommons.org/licenses/by/3.0>), which permits unrestricted use, distribution, and reproduction in any medium, provided the original work is properly cited. 

References

- [1] Lvovsky AI, Sanders BC, Tittel W. Optical quantum memory. *Nature Photonics*. 2009;3:706-714
- [2] Bloch I. Quantum coherence and entanglement with ultracold atoms in optical lattices. *Nature*. 2008;453:1016
- [3] Saffman M, Walker TG. Analysis of a quantum logic device based on dipole-dipole interactions of optically trapped Rydberg atoms. *Physical Review A*. 2005;72:022347
- [4] Specht HP, Nölleke C, Reiserer A, Uphoff M, Figueroa E, Ritter S, et al. A single-atom quantum memory. *Nature*. 2011;473:190-193
- [5] Negretti A, Treutlein P, Calarco T. Quantum computing implementations with neutral particles. *Quantum Information Processing*. 2011;10:721
- [6] Weitenberg C, Kuhr S, Mølmer K, Sherson JF. Quantum computation architecture using optical tweezers. *Physical Review A*. 2011;84:032322
- [7] Ritter S et al. An elementary quantum network of single atoms in optical cavities. *Nature*. 2012;484:195
- [8] Hofmann J et al. Heralded entanglement between widely separated atoms. *Science*. 2012;337:72
- [9] Duan LM, Monroe C. Colloquium: Quantum networks with trapped ions. *Reviews of Modern Physics*. 2010;82:1209
- [10] Chen S et al. Deterministic and storable single-photon source based on a quantum memory. *Physical Review Letters*. 2006;97:173004
- [11] Chen Y-A et al. Memory-built-in quantum teleportation with photonic and atomic qubits. *Nature Physics*. 2008;4:103
- [12] Grimm R et al. Optical dipole traps for neutral atoms. *Advances in Atomic, Molecular, and Optical Physics*. 2000;42:95
- [13] Davidson N et al. Long atomic coherence times in an optical dipole trap. *Physical Review Letters*. 1995;74:1311
- [14] Lengwenus A, Kruse J, Volk M, Ertmer W, Birkl G. Coherent manipulation of atomic qubits in optical micropotentials. *Applied Physics B*. 2007;86:377
- [15] Miller JD, Cline RA, Heinzen DJ. Far-off-resonance optical trapping of atoms. *Physical Review A*. 1993;47:R4567
- [16] Schlosser N, Reymond G, Protsenko I, Grangier P, Schlosser N, Reymond G, et al. Sub-poissonian loading of single atoms in a microscopic dipole trap. *Nature*. 2001;411:1024
- [17] Volz J, Weber M, Schlenk D, Rosenfeld W, Kurtsiefer C, Weinfurter H. An atom and a photon. *Laser Physics*. 2007;17:1007
- [18] Puppe T, Schuster I, Grothe A, Kubanek A, Murr K, Pinkse PWH, et al. Trapping and observing single atoms in a blue-detuned intracavity dipole trap. *Physical Review Letters*. 2007;99:013002
- [19] Nelson KD, Li X, Weiss DS. Imaging single atoms in a three-dimensional array. *Nature Physics*. 2007;3:556
- [20] Phoonthong P, Douglas P, Wickenbrock A, Renzoni F. Characterization of a state-insensitive dipole trap for cesium atoms. *Physical Review A*. 2010;82:013406
- [21] Weber M, Volz J, Saucke K, Kurtsiefer C, Weinfurter H. Analysis of

a single-atom dipole trap. *Physical Review A*. 2006;**73**:043406

[22] Schlosser N, Reymond G, Protsenko I, Grangier P. Sub-poissonian loading of single atoms in a microscopic dipole trap. *Nature*. 2001;**411**:1024-1027

[23] Zoller P. Quantum optics: Tricks with a single photon. *Nature*. 2000;**404**:340-341

[24] Khudaverdyan M, Alt W, Dotsenko I, Kampschulte T, Lenhard K, Rauschenbeutel A, et al. Controlled insertion and retrieval of atoms coupled to a high-finesse optical resonator. *New Journal of Physics*. 2008;**10**:073023

[25] Blinov BB, Moehring DL, Duan LM, Monroe C. Observation of entanglement between a single trapped atom and a single photon. *Nature*. 2004;**428**:153-157

[26] Dudin YO, Li L, Kuzmich A. Light storage on the minute scale. *Physical Review A*. 2013;**87**:031801

[27] Li L, Kuzmich A. Quantum memory with strong and controllable Rydberg-level interactions. *Nature Communications*. 2016;**7**:13618

[28] Saffman M, Walker TG, Mølmer K. Quantum information with Rydberg atoms. *Reviews of Modern Physics*. 2010;**82**:2313

[29] Jaksch D et al. Fast quantum gates for neutral atoms. *Physical Review*. 2000;**85**:2208

[30] Choi JH, Knuffman B, Leibisch TC, Reinhard A, Raithel G. Cold Rydberg atoms. *Advances in Atomic, Molecular, and Optical Physics*. 2007;**54**:131

[31] Jaksch D, Cirac JI, Zoller P, Rolston SL, Côté R, Lukin MD. Fast quantum gates for neutral atoms. *Physical Review Letters*. 2000;**85**:2208

[32] Heidemann UR, Bendkowsky V, Butscher B, Löw R, Santos L, Pfau T. Evidence for coherent collective Rydberg excitation in the strong blockade regime. *Physical Review Letters*. 2007;**99**:163601

[33] Gaëtan A, Evellin C, Wolters J, Grangier P, Wilk T, Browaeys A. Analysis of the entanglement between two individual atoms using global Raman rotations. *New Journal of Physics*. 2010;**12**:065040

[34] Firstenberg O, Adams CS, Hofferberth S. Nonlinear quantum optics mediated by Rydberg interactions. *Journal of Physics B: Atomic, Molecular and Optical Physics*. 2016;**49**:152003

[35] Mohapatra AK et al. A giant electro-optic effect using polarizable dark states. *Nature Physics*. 2008;**4**:890

[36] Isenhower L, Saffman M, Mølmer K. Multibit Ck NOT quantum gates via Rydberg blockade. *Quantum Information Processing*. 2011;**10**:755

[37] Muller MM, Murphy M, Montangero S, Calarco T, Grangier P, Browaeys A. Implementation of an experimentally feasible controlled-phase gate on two blockaded Rydberg atoms. *Physical Review A*. 2014;**89**:032334

[38] Das S, Grankin A, Iakoupov I, Brion E, Borregaard J, Boddeda R, et al. Photonic controlled-PHASE gates through Rydberg blockade in optical cavities. *Physical Review A*. 2016;**93**:040303(R)

[39] Peyronel T, Firstenberg O, Liang Q, Hofferberth S, Gorshkov A, Pohl T, et al. Quantum nonlinear optics with single photons enabled by strongly interacting atoms. *Nature*. 2012;**488**:57

[40] Pritchard JD, Maxwell D, Gauguet A, Weatherill KJ, Jones MPA, Adams

- CS. Cooperative atom-light interaction in a blockaded Rydberg ensemble. *Physical Review Letters*. 2010;**105**:193603
- [41] Pritchard JD, Weatherill KJ, Adams CS. Nonlinear quantum optics mediated by Rydberg interactions. In: Madison KW et al., editors. *Annual Review of Cold Atoms and Molecules*. Vol. 1. 2013. pp. 301-350
- [42] Kozhekin AE, Mølmer K, Polzik E. Quantum memory for light. *Physical Review A*. 2000;**62**:033809
- [43] Müller MM, Haakh HR, Calarco T, Koch CP, Henkel C. Prospects for fast Rydberg gates on an atom chip. *Quantum Information Processing*. 2011; **10**:771
- [44] Beijersbergen M, Coerwinkel R, Kristensen M, Woerdman J. Helical-wavefront laser beams produced with a spiral phaseplate. *Optics Communications*. 1994;**112**:321
- [45] Curtis JE, Koss BA, Grier DG. Molecular distributed sensors using dark soliton array trapping tools. *Optics Communications*. 2002;**207**:169
- [46] Mirhosseini M, na Loaiza OSM, Chen C, Rodenburg B, Malik M, Boyd RW. Rapid generation of light beams carrying orbital angular momentum. *Optics Express*. 2013;**21**:30196
- [47] Beijersbergen M, Allen L, van der Veen H, Woerdman J. Astigmatic laser mode converters and transfer of orbital angular momentum. *Optics Communications*. 1993;**96**:123
- [48] Wang J et al. Terabit free-space data transmission employing orbital angular momentum multiplexing. *Nature Photonics*. 2012;**6**(7):488-496
- [49] Allen L et al. Orbital angular-momentum of light and the transformation of Laguerre-Gaussian laser modes. *Physical Review A*. 1992; **45**(11):8185-8189
- [50] Mashhadi L, Mehrafarin M. Paraxial propagation in amorphous optical media with screw dislocation. *Journal of Optics*. 2010;**12**:035703
- [51] Berry M. Paraxial beams of spinning light. *Proceedings of SPIE*. 1998;**3487**:6
- [52] Allen L et al. Atom dynamics in multiple Laguerre-Gaussian beams. *Physical Review A*. 1996;**54**(5):4259-4270
- [53] Jáuregui R. Rotational effects of twisted light on atoms beyond the paraxial approximation. *Physical Review A*. 2004;**70**:033415-033411-033419
- [54] Babiker M et al. Orbital angular momentum exchange in the interaction of twisted light with molecules. *Physical Review Letters*; **89**(14):143601
- [55] Van Enk JK. Selection rules and center of mass motion of ultra cold atoms. *Quantum Opt*. 1994;**6**:445-457
- [56] Alexandrescu A et al. Electronic and centre of mass transitions driven by Laguerre-Gaussian beams. *Journal of Optics B: Quantum and Semiclassical Optics*. 2005;**7**:87-92
- [57] Kumar Mondal P, Deb B, Majumder S. Angular momentum transfer in interaction of Laguerre-Gaussian beams with atoms and molecules. *Physical Review A*. 2014;**89**:063418
- [58] Muthukrishnan A, Stroud CR Jr. Entanglement of internal and external angular momenta of a single atom. *Journal of Optics B: Quantum and Semiclassical Optics*. 2002;**4**:S73-S77
- [59] Krenn M, Malik M, Erhard M, Zeilinger A. Orbital angular momentum of photons and the entanglement of Laguerre-Gaussian modes. *Philosophical*

Transactions of the Royal Society A. 2017;**375**(2087):20150442

[60] Isenhower L, Williams W, Dally A, Saffman M. Atom trapping in an interferometrically generated bottle beam trap. *Optics Letters*. 2009; **34**:1159

[61] Ng J, Lin Z, Chan CT. Theory of optical trapping by an optical vortex beam. *Physical Review Letters*. 2010; **104**:103601

[62] Miroshnychenko Y et al. Coherent excitation of a single atom to a Rydberg state. *Physical Review A*. 2010;**82**: 013405

[63] Fahey DP, Michael W. Noel excitation of Rydberg states in rubidium with near infrared diode laser. *Optics Express*. 2011;**19**:17002

[64] Johnson LAM, Majeed HO, Varcoe BTH. *Applied Physics B: Lasers and Optics*. 2012;**106**:257

[65] Fahey DP, Noel MW. Excitation of Rydberg states in rubidium with near infrared diode lasers. *Optics Express*. 2011;**19**:17002

[66] Sheng J, Chao Y, Kumar S, Fan H, Sedlacek J, Shaffer JP. Intracavity Rydberg-atom electromagnetically induced transparency using a high-finesse optical cavity. *Physical Review A*. 2017;**96**:033813

[67] Johnson LAM, Majeed HO, Sanguinetti B, Becker T, Varcoe BTH. Absolute frequency measurements of $85\text{Rb}nF/2$ Rydberg states using purely optical detection. *New Journal of Physics*. 2010;**12**:063028

[68] Johnson TA, Urban E, Henage T, Isenhower L, Yavuz DD, Walker TG, et al. Rabi oscillations between ground and Rydberg states with dipole-dipole

atomic interactions. *Physical Review Letters*. 2008;**100**:113003

[69] Keating T, Cook RL, Hankin AM, Jau Y-Y, Biedermann GW, Ivan H. Deutsch Robust quantum logic in neutral atoms via adiabatic Rydberg dressing. *Physical Review A*. 2015;**91**: 012337

[70] Ryabtsev II, Beterov II, Tretyakov DB, Entin VM, Yakshina EA, Rzhanov AV. Doppler- and recoil-free laser excitation of Rydberg states via three-photon transitions. *Physical Review A*. 2011;**84**:053409

[71] Baur S, Tiarks D, Rempe G, Dürr S. Single-photon switch based on Rydberg blockade. *Physical Review Letters*. 2014; **112**:073901

[72] Heckötter J, Freitag M, Fröhlich D, Aßmann M, Bayer M, Semina MA, et al. Scaling laws of Rydberg excitons. *Physical Review B*. 2017;**96**:125142

[73] Niederprüm T, Thomas O, Manthey T, Weber TM, Ott H. Giant cross section for molecular ion formation in ultracold Rydberg gases. *Physical Review Letters*. 2015;**115**:013003

[74] Safronova MS, Williams CJ, Clark CW. Frequency-dependent polarizabilities of alkali atoms from ultraviolet through infrared spectral regions. *Physical Review A*. 2003;**67**: 040303

[75] Piotrowicz MJ, Lichtman M, Maller K, Li G, Zhang S, Isenhower L, et al. Two-dimensional lattice of blue-detuned atom traps using a projected Gaussian beam array. *Physical Review A*. 2013;**88**:013420

[76] Zhang S, Robicheaux F, Saffman M. Magic-wavelength optical traps for Rydberg atoms. *Physical Review A*. 2011;**84**:043408

[77] Mashhadi L. Three-photon Gaussian–Gaussian–Laguerre–Gaussian excitation of a localized atom to a highly excited Rydberg state. *Journal of Physics B: Atomic, Molecular and Optical Physics*. 2017;**50**:245201

[78] Curtis JE, Grier DG. Structure of optical vortices. *Physical Review Letters*. 2003;**90**:133901

[79] Lembessis VE, Babiker M. Enhanced quadrupole effects for atoms in optical vortices. *Physical Review Letters*. 2013;**110**:083002

[80] Allen L, Babiker M, Powerb WL. Azimuthal Doppler shift in light beams with orbital angular momentum. *Optics Communication*; **112**:141

[81] Blum K. *Density Matrix Theory and Applications*. New York: Plenum Press; 1981

[82] Seaton MJ. The quantum defect method. *Monthly Notices of the Royal Astronomical Society*. 1958;**118**:504

[83] Kreuter A, Becher C, GPT L, Mundt AB, Russo C, Häffner H, et al. Experimental and theoretical study of the 3d2D-level lifetime of 40Ca⁺. *Physical Review A*. 2005;**71**:032504